Inorg. Chem. **2003**, *42*, 273–282

Intramolecular Excimer Formation in a Naphthalene-Appended Dinuclear Iron–Oxo Complex

Laura B. Picraux,[†] Brandon T. Weldon,[†] and James K. McCusker*

Department of Chemistry, Michigan State University, East Lansing, Michigan 48824

Received September 23, 2002

The synthesis, structure, and physical properties of a Heisenberg exchange-coupled cluster containing naphthalene groups are described. $[Fe_2(O)(O_2CCH_2C_{10}H_7)_2(TACN\text{-}Me_3)_2]^{2+}$ (**3**) crystallizes in space group $P\bar{1}$ with unit cell parameters $a = 12.94(2)$ Å, $b = 14.84(2)$ Å, $c = 15.23(2)$ Å, $\alpha = 101.12(7)°$, $\beta = 90.8(1)°$, $\gamma = 114.14(7)°$, $V = 2605(6)$ Å^3, and $Z = 2$ with $R = 0.0425$ and wR2 = 0.1182. Variable-temperature magnetic susceptibility data indicate that the two high-spin Fe^{III} centers are antiferromagnetically coupled with $J = -105$ cm^{-1} ($\mathbf{H} = -2J\mathbf{S}_1\cdot\mathbf{S}_2$), which is typical for this class of compounds. The room-temperature static emission spectrum of the compound in deoxygenated CH_3CN solution is centered near 335 nm and has features reminiscent of both methyl-2-naphthylacetate (**1**) and $[Zn_2(OH)(O_2CCH_2C_{10}H_7)_2(TACN\text{-}Me_3)_2]^+$ (**2**) with the following two caveats: (1) the overall emission intensity is roughly a factor of 10 less than that of the free ester (**1**, $\Phi_r = 0.13$) or the Zn^{II} analogue (**2**, $\Phi_r = 0.14$), and (2) there is significant broadening of the low-energy shoulder of the emission envelope. Time-correlated single photon counting data revealed biphasic emission for **3** with $\tau_1 = 4.6 \pm 1$ ns and $\tau_2 = 47 \pm 1$ ns. The latter compares favorably with that found for **2** ($\tau = 47 \pm 1$ ns) and is assigned as the $S_0 \leftarrow S_1$ fluorescence of naphthalene. Emission anisotropy, time-gated emission spectra, and nanosecond time-resolved absorption measurements all support the assignment of the 4.6 ns component as being due to a singlet excimer that forms between the two naphthylacetate groups of **3**, a process that is likely mediated by the structural constraints of the oxo-bis-carboxylato diiron core. No direct evidence for intramolecular electron and/or energy transfer from the photoexcited naphthyl group to the iron–oxo core was obtained, suggesting that the short-lived excimer may contribute to circumventing such pathways in this type of system.

Introduction

Heisenberg spin coupling is an important feature of the electronic structure of molecules possessing two or more paramagnetic components. Manipulation of this interaction is central to the emerging area of molecular magnetic materials,[1−3] and its characterization has played a key role in the development of the field of magnetochemistry in general.[4] Spin coupling is also manifest in bioinorganic chemistry in that the electronic structures of polymetallic active sites reflect exchange interactions within the metal cluster cores.[5,6] Whereas the occurrence and mechanistic details of Heisenberg spin coupling have been vigorously pursued, the notion of its influence on the chemistry exhibited by a given system has received little attention. Reports by a number of workers provide both direct[7−13] and indirect[14,15]

* To whom correspondence should be addressed. E-mail: mccusker@cem.msu.edu.

[†] Department of Chemistry, University of California at Berkeley.

(1) Kahn, O. *Acc. Chem. Res.* **2000**, *33*, 1.
(2) Kahn, O.; Martinez, C. J. *Science* **1998**, *279*, 44.
(3) Miller, J. H.; Mallard, W. G.; Smyth, K. C. *J. Phys. Chem.* **1984**, *88*, 4963−4970.
(4) Kahn, O. *Molecular Magnetism*; VCH Publishers: New York, 1993.
(5) Holm, R. H.; Kennepohl, P.; Solomon, E. I. *Chem. Rev.* **1996**, *96*, 2239−2314.
(6) Lippard, S. J.; Berg, J. M. *Principles of Bioinorganic Chemistry*; University Science Books: Mill Valley, CA, 1994.
(7) Blondin, G.; Girerd, J.-J. *Chem. Rev.* **1990**, *90*, 1359.
(8) Bersuker, I. B.; Borshch, S. A. *Adv. Chem. Phys.* **1992**, 703.
(9) Achim, C.; Bominaar, E. L.; Munck, E. *J. Biol. Inorg. Chem.* **1998**, *3*, 126.
(10) Achim, C.; Bominaar, E. L.; Staples, R. J.; Munck, E.; Holm, R. H. *Inorg. Chem.* **2001**, *40*, 4389−4403.
(11) Bominaar, E. L.; Achim, C.; Borshch, S. A. *J. Chem. Phys.* **1999**, *110*, 11411.
(12) Bertrand, P.; Gayda, J.-P. *Biochim. Biophys. Acta* **1982**, *680*, 331.
(13) Mouesca, J. M.; Chen, J.-P.; Noodleman, L.; Bashford, D.; Case, D. A. *J. Am. Chem. Soc.* **1994**, *116*, 11898.
(14) Macatangay, A. V.; Endicott, J. F.; Song, X. *J. Phys. Chem. A* **1998**, *102*, 7537−7540.
(15) Brunold, T. C.; Gamelin, D. R.; Solomon, E. I. *J. Am. Chem. Soc.* **2000**, *122*, 8511−8523.

10.1021/ic026054m CCC: $25.00
Published on Web 12/24/2002

theoretical support for a possible correlation between spin exchange and chemical reactivity: however, experimental evidence along these lines is limited.[16] Several years ago, we therefore initiated a program to study this issue in the context of electron and energy transfer reactions.

In the course of this work, we have exploited the oxo-bis-carboxylato dinuclear Fe(III) class of complexes. These compounds provide a convenient platform due in large part to the ease with which spin coupling within the dinuclear core can be modulated. For example, protonation of $Fe_2O(O_2CCH_3)_2(Tp)_2$ (where Tp is hydrotris(pyrazolyl)borate) affords the corresponding OH-bridged complex in which the exchange interaction between the two high-spin Fe^{III} centers is attenuated by nearly a factor of 10.[17−19] We have used this system as the basis for a detailed study of the bimolecular reactivity of exchange-coupled complexes.[20] This work was successful in demonstrating that changes in driving force and reorganization energy could not account for the substantial difference in the reactivity observed between the oxo- (strong coupling) and hydroxo- (weak coupling) bridged complexes. Unfortunately, electron transfer from the photoexcited Ru^{II} donors to the hydroxo-bridged dinuclear clusters was diffusion-limited. Only a lower limit for the rate difference was therefore obtained, and a correlation between reactivity and electron exchange coupling could not be established.

The obvious (though synthetically more challenging) solution to this problem requires complex assemblies in which the donor is covalently linked to the exchange-coupled complex. Electron and/or energy transfer events then become an intramolecular process and not subject to the kinetic limitations of diffusion. While a variety of structural motifs are possible, one of the more straightforward assemblies involves appending the donor to the metal cluster through the bridging carboxylates. Herein, we report the synthesis and characterization of such a compound, $[Fe_2O(O_2CCH_2C_{10}H_7)_2(TACN\text{-}Me_3)_2]^{2+}$, which contains naphthalene as a potential donor to the exchange coupled diiron(III) core.

Experimental Section

General. All reagents were obtained from commercial sources and used without further purification. The TACN-Me_3 (where TACN-Me_3 is 1,4,7-trimethyl-1,4,7-triazacyclononane) was donated by Professor Jeffrey Long of the University of California, Berkeley. The compound $(TACN\text{-}Me_3)FeCl_3$ was prepared according to literature procedures.[21] Elemental analyses and mass spectra (standard FAB conditions) were obtained through the analytical facilities at Michigan State University. ^1H and ^{13}C spectra were recorded on a Varian INOVA 300 MHz spectrometer.

Methyl-2-Naphthylacetate (1). A solution of 2-naphthylacetic acid (500 mg, 2.69 mmol) in 15 mL of methanol with 0.25 mL of hydrochloric acid was brought to and maintained at reflux for 24 h. The solvent was reduced to 5 mL, and the solution was neutralized with 20 mL of a saturated sodium bicarbonate solution. The ester was extracted with dichloromethane (3 × 15 mL), dried over sodium sulfate, and concentrated to dryness to produce a colorless oil in quantitative yield. ^1H NMR ($CDCl_3$): δ 7.85−7.81 (m, 3 H), 7.75 (s, 1 H), 7.50−7.42 (m, 3 H), 3.82 (s, 2 H), 3.73 (s, 3 H). ^{13}C NMR ($CDCl_3$): δ 176.9, 133.7, 132.8, 131.7, 128.5, 128.2, 127.9, 127.6, 126.4, 126.1, 52.4, 41.6. Anal. Calcd for $C_{13}H_{12}O_2$: C, 77.98; H, 6.04. Found: C, 77.99; H, 6.22. Electronic absorption spectrum (in CH_3CN at 298 K) λ, nm (ϵ, M^{-1} cm^{-1}): 268 (4820), 276 (5090), 286 (3410).

$[Zn_2(OH)(O_2CCH_2C_{10}H_7)_2(TACN\text{-}Me_3)_2](ClO_4)$ (2). This compound was synthesized by a modification of a method previously described in the literature.[22] A flask was charged with 217 mg (0.584 mmol) of $ZnClO_4 \cdot 6H_2O$ in 10 mL of ethanol. To this vigorously stirring solution was added dropwise 5 mL of an ethanol solution containing 109 mg (0.584 mmol) of 2-naphthylacetic acid and 59 mg (0.58 mmol) of triethylamine. A white precipitate formed upon addition of the acid. The mixture was stirred for 2 h, at which time 100 mg (0.584 mmol) of TACN-Me_3 in 5 mL of ethanol was added dropwise. The resultant mixture was stirred for 2 h followed by addition of 5 mL of methanol to facilitate dissolution of the precipitate. The solution was stirred for an additional 2 h. The reaction mixture was allowed to cool in an ice bath for 1 h and then filtered to yield analytically pure product (yield: 37%). X-ray quality crystals were grown from an acetonitrile solution stored at −20 °C for several days (the compound was not dried prior to crystallization which resulted in retention of a CH_3OH solvate as evidenced by the X-ray structure). ^1H NMR ($CDCl_3$): δ 7.88−7.80 (m, 6 H), 7.72 (s, 2 H), 7.51−7.41 (m, 6 H), 3.68 (s, 4 H), 2.62−2.44 (m, 19 H), 2.39−2.29 (m, 23 H), 2.22 (s, 9 H). Anal. Calcd for $C_{42}H_{61}N_6O_9Zn_2Cl$: C, 52.54; H, 6.40; N, 8.75. Found: C, 52.52; H, 6.02; N, 8.63. MS (FAB): *m/z* 860 ($[M - ClO_4]^+$). Electronic absorption spectrum (in CH_3CN at 298 K) λ, nm (ϵ, M^{-1} cm^{-1}): 278 (1650), 284 (1700), 292 (1100).

$[Fe_2(O)(O_2CCH_2C_{10}H_7)_2(TACN\text{-}Me_3)_2](PF_6)_2$ (3). The synthesis of this compound was based on methods already developed in the literature.[23] To a stirring suspension of 300 mg (0.890 mmol) of $(TACN\text{-}Me_3)FeCl_3$ in 10 mL of ethanol was added 168 mg (0.900 mmol) of 2-naphthylacetic acid and 91 mg (0.90 mmol) of triethylamine in 5 mL of ethanol dropwise. The resulting solution immediately turned brown in color and was allowed to stir overnight. The solution was filtered, and 1 g (6 mmol) of solid NH_4PF_6 was added to the filtrate. The mixture was stirred for 10 min, filtered, and then dried to give analytically pure product (yield: 30%). X-ray quality crystals were grown by slow evaporation of a CH_2Cl_2 solution of the compound at −20 °C. Anal. Calcd for $C_{40}H_{60}N_6O_5Fe_2P_2F_{12}$: C, 42.49; H, 5.35; N, 7.43. Found: C, 42.56; H, 5.32; N, 7.32. Electronic absorption spectrum (in CH_3CN at 298 K) λ, nm (ϵ, M^{-1} cm^{-1}): 268 (16 800), 276 (15 200), 286 (10 600), 348 (7250), 478 (1420), 522 (1100), 726 (160).

Physical Measurements: X-ray Structure Determinations. Single-crystal X-ray diffraction data for $[Zn_2(OH)(O_2CCH_2C_{10}H_7)_2(TACN\text{-}Me_3)_2](ClO_4)$ (**2**) and $[Fe_2(O)(O_2CCH_2C_{10}H_7)_2(TACN\text{-}Me_3)_2](PF_6)_2$ (**3**) were collected on a Siemens SMART diffractometer equipped with an Oxford Cryosystems low-temperature device at the X-ray facility of Michigan State University. Crystal-

(16) Monzyk, M. M.; Holwerda, R. A. *Inorg. Chem.* **1992**, *31*, 1969−1971.
(17) Armstrong, W. H.; Lippard, S. J. *J. Am. Chem. Soc.* **1983**, *105*, 4837.
(18) Armstrong, W. H.; Lippard, S. J. *J. Am. Chem. Soc.* **1984**, *106*, 4632.
(19) Rodriguez, J. H.; McCusker, J. K. *J. Chem. Phys.* **2002**, *116*, 6253.
(20) Weldon, B. T.; Wheeler, D. E.; Kirby, J. P.; McCusker, J. K. *Inorg. Chem.* **2001**, *40*, 6802−6812.
(21) Wieghardt, K.; Pohl, K.; Gerbert, W. *Angew. Chem., Int. Ed. Engl.* **1983**, *22*, 727.
(22) Chaudhuri, P.; Claudia, S.; Wieghardt, K.; Deck, W.; Gregorzik, R.; Vahrenkamp, H.; Nuber, B.; Weiss, J. *Inorg. Chem.* **1992**, *31*, 1451−1457.
(23) Hartman, J. R.; Rardin, R. L.; Chaudhuri, P.; Pohl, K.; Wieghardt, K.; Nuber, B.; Weiss, J.; Papaefthymiou, G. C.; Frankel, R. B.; Lippard, S. J. *J. Am. Chem. Soc.* **1987**, *109*, 7387−7396.

Table 1. Crystallographic Data for $[Zn_2(OH)(O_2CCH_2C_{10}H_7)_2(TACN\text{-}Me_3)_2](ClO_4)\cdot CH_3OH$ (**2**) and $[Fe_2(O)(O_2CCH_2C_{10}H_7)_2(TACN\text{-}Me_3)_2](PF_6)_2\cdot CH_2Cl_2$ (**3**)

	2	**3**
empirical formula	$C_{43}H_{65}N_6ClO_{10}Zn_2$	$C_{43}H_{62}N_6Cl_2F_{12}Fe_2O_5P_2$
fw	988.17	1215.53
cryst color, habit	colorless, blocks	brown/green, blocks
cryst syst	monoclinic	triclinic
space group	$P2_1/c$	$P\bar{1}$
temp (K)	173(2)	173(2)
cell dimensions		
a (Å)	18.361(3)	12.944(16)
b (Å)	13.290(2)	14.843(15)
c (Å)	19.450(3)	15.23(2)
α (deg)	90	101.12(7)
β (deg)	101.553(3)	90.81(10)
γ (deg)	90	114.14(7)
V (Å^3)	4649.9(13)	2605(6)
Z	4	2
D_{calcd} (g cm^{-3})	1.412	1.549
GOF (F^2)	0.816	0.507
R^a	0.0280	0.0425
wR2^b	0.0916	0.1182

^{a} $R = \sum||F_o| - |F_c||/\sum|F_o|$. ^{b} $wR2 = \{\sum[w(F_o^2 - F_c^2)^2]/\sum[w(F_o^2)^2]\}^{1/2}$.

lographic data are summarized in Table 1. Lattice parameters were obtained from least-squares analyses. Crystals showed no significant decay during the data collection. Data were integrated (SAINT),[24] corrected for Lorentz and polarization effects, and analyzed for agreement and possible absorption (SADABS) using XPREP.[25] Space group assignments were based on systematic absences, packing considerations, a statistical analysis of intensity distribution, and successful refinement of the structure. The structures were solved by direct methods and expanded using Fourier techniques. All structure calculations were performed with the SHELXTL 5.1 software package.[25] For **2**, all non-hydrogen atoms were refined anisotropically; the hydrogen atoms were included in calculated positions, but not refined. For **3**, all non-hydrogen atoms were refined anisotropically. The hydrogen atoms were located in the difference electron density map and refined accordingly. Further details concerning the structure determinations are deposited as Supporting Information.

Cyclic Voltammetry. Electrochemical measurements were carried out in a dinitrogen-filled drybox (Vacuum Atmospheres) using a BAS CV-50W electrochemical analyzer. A standard three-electrode configuration was employed consisting of Pt working and counter electrodes and $Ag/AgNO_3$ as the reference. Compounds were dissolved in CH_3CN that was 0.1 M in NBu_4PF_6; the CH_3CN had been passed over a silica column and distilled first from $KMnO_4$ and then from CaH_2. All measurements were made on solutions containing trace amounts of ferrocene to allow for internal calibration of the observed potentials.

Variable-Temperature Magnetic Susceptibility. Magnetic susceptibility data were collected using a Quantum Design MPMS SQUID magnetometer interfaced to an IBM PC. Data were collected in an applied field of 1 T. Following each temperature change, the system was kept at the new temperature for an additional 5 min before data collection to ensure thermal equilibration of the sample. Data were corrected for diamagnetism of the sample using Pascal's constants and for the measured susceptibility of the sample holder and reported herein as effective magnetic moments. Data were fit to the van Vleck equation using Magfit.[26] Solution susceptibility measurements at room temperature were made via the Evans NMR method using a Varian 300 MHz spectrometer. The shift of the *tert*-butyl alcohol CH_3 resonance in a 10% *tert*-butyl alcohol/CD_3CN solution was used to determine $\Delta\nu$.

Electronic Absorption and Static Emission Measurements. All spectroscopic data were obtained on samples in sealed cells and dissolved in CH_3CN that had been passed over a silica column, doubly distilled (from $KMnO_4$ then CaH_2), and stored under an inert atmosphere. Static electronic absorption spectra were recorded using a Hewlett-Packard 8452A diode array spectrophotometer. Static emission spectra were acquired using a Spex FluoroMax fluorimeter. Emission spectra were corrected for instrumental response by using a NIST standard of spectral irradiance (Optronic Laboratories, Inc., OL220M tungsten quartz lamp). All subsequent data manipulations were carried out with the corrected spectra as described elsewhere.[27]

Radiative quantum yields (Φ_r) were determined relative to triphenylene ($\Phi_r = 0.065$ in ethanol[28,29]) which had been purified by recrystallization from hexanes. Measurements were carried out on optically thin solutions (OD $\sim$ 0.05). The samples were prepared in an Ar atmosphere drybox in 1 cm path length sealed quartz cuvettes. Quantum yields were calculated according to the following equation:

$$\Phi_{unk} = \Phi_{std}\cdot\left(\frac{I_{unk}/A_{unk}}{I_{std}/A_{std}}\right)\cdot\left(\frac{\eta_{unk}}{\eta_{std}}\right)^2 \quad (1)$$

where Φ_{unk} and Φ_{std} are the radiative quantum yields of the sample and the standard, I_{unk} and I_{std} are the integrated emission intensities of the sample and standard, A_{unk} and A_{std} are the absorbances of the sample and standard at the excitation wavelength (254 nm), and η_{unk} and η_{std} are the indices of refraction of the sample and standard solutions (taken to be equivalent to neat CH_3CN and EtOH, respectively).

Time-Correlated Single-Photon Counting Emission Spectroscopy (TCSPC). The apparatus used for acquisition of emission data via TCSPC is described elsewhere.[30] Briefly, a mode-locked Ar-ion laser was used to synchronously pump a dye laser charged with pyromethane 567. The 280 nm light used for excitation was obtained by doubling the 560 nm dye output in a KDP type I second harmonic crystal. For routine lifetime and gated spectra measurements, emission polarization was detected at the magic angle (54.7°) relative to the excitation polarization. Samples (OD $\sim$ 0.05) were sealed under Ar in a 1 cm path length quartz cuvette, and the emission was monitored from 320 to 400 nm in 10 nm increments (5 nm band-pass). The measured instrument response function was ca. 30 $\pm$ 5 ps (fwhm); data were collected over 1064 channels corresponding to a time window of 100 ns.

Lifetimes were determined by fitting the data using the Microcal Origin 6.0 software package.[31] Because of the density of data points in the 100 ns window, data were fit for delay times $\Delta t \geq 1$ ns. Compounds **1** and **2** could each be fit to single exponential decays at all wavelengths monitored. Compound **3** required two exponentials at all wavelengths in order to obtain reasonable fits. As

(24) *SAINT+*, 6.02 ed.; Bruker AXS: Madison, WI, 1999.
(25) *XPREP*, 5.1 ed.; Siemens Industrial Automation, Inc.: Madison, WI, 1995.
(26) Schmitt, E. Ph.D. Dissertation. Department of Chemistry, University of Illinois, Urbana-Champaign, IL, 1996.
(27) Damrauer, N. H.; Boussie, T. R.; Devenney, M.; McCusker, J. K. *J. Am. Chem. Soc.* **1997**, *119*, 8253−8268.
(28) Dawson, W. R.; Windsor, M. W. *J. Phys. Chem.* **1968**, *72*, 3251−3260.
(29) The ethanol was distilled over 4 Å molecular sieves and stored under an inert atmosphere prior to use.
(30) DeWitt, L.; Blanchard, G. J.; LeGoff, E.; Benz, M. E.; Liao, J. H.; Kanatzidis, M. G. *J. Am. Chem. Soc.* **1993**, *115*, 12158−12164.
(31) *Microcal Origin*, 6.0 ed.; Microcal Software, Inc.: Northampton, MA, 1991−1999.

evidenced by the gated spectra (vide infra), the two decay components are characterized by distinct emission profiles. Thus, accurate values for the two time constants were determined by first focusing on the data collected at 320 nm (where the amplitude of the longer time component is largest) and 400 nm (where the amplitude of the shorter time component dominates). The data were analyzed by an iterative process in which the decay at 320 nm (τ_2) was fit while keeping the value of τ_1 fixed. This value of τ_2 was then held constant for determining τ_1 at 400 nm and so on. This cycle was repeated until the two time constants converged on their final values. All other wavelengths between 320 and 400 nm were fit by holding both τ_1 and τ_2 constant at their converged values and allowing the preexponential factors to freely vary.[32] Satisfactory fits of emission decay at all probe wavelengths were obtained in this manner.

Spectral profiles corresponding to the two emissive components of **3** were obtained by first fitting the single-wavelength decays as already detailed. The fitted amplitudes were then normalized to the known emission profile of compound **1**. This was accomplished by obtaining single-wavelength decay data for **1** in the range 320−400 nm and normalizing these decay amplitudes to the compound's corrected static emission spectrum. This created an effective correction factor for each emission probe wavelength that was then applied to the data on compounds **2** and **3**, allowing for a direct comparison between the gated emission spectra and the static emission spectra for all three compounds.

Polarized emission data were acquired at 360 nm (20 nm bandpass) following excitation at 280 nm. The anisotropy, $r(t)$, was computed according to the following relation:

$$r(t) = (I_{||} - I_{\perp})/(I_{||} + 2I_{\perp}) \quad (2)$$

where $I_{||}$ and $I_{\perp}$ are the emission data collected parallel and perpendicular to the excitation polarization, respectively. The resulting curve was fit to an exponential decay model. The amplitudes of the fits were taken as $r(0)$

$$r(0) = {}^1/_5(3\cos^2\delta - 1) \quad (3)$$

where δ is the relative angle between the emissive and absorptive (i.e., excitation) transition dipoles.

Time-Resolved Electronic Absorption Spectroscopy. Nanosecond time-resolved absorption measurements were carried out using a Nd:YAG-based laser spectrometer described elsewhere.[27] Each sample was dissolved in CH_3CN (purified as already described) with an absorbance of ~1 (1 cm path length) at the excitation wavelength of 266 nm and sealed under an Ar atmosphere in a quartz cuvette. The data correspond to a 60 shot average (0.5 Hz) of the signal and baseline as well as background sample emission with 1.3 mJ of power at the sample; the baseline and emission were subsequently subtracted from the signal and the data analyzed using programs of local origin. The sample was monitored for decomposition by irradiating it under experimental conditions and monitoring the ground-state and transient electronic absorption every 15 min. These data suggested that the sample begins to decompose after 3 h of irradiation. A fresh sample was therefore prepared every 2 h to ensure that the integrity of the sample was maintained throughout data acquisition.

Molecular Mechanics Simulations. Calculations on compounds **2** and **3** were carried out using the Spartan 5.0 software package.[33] The crystal structure for each compound was used as a starting point; that is, no geometry optimization was performed. The molecular mechanics MMFF94 model was used for all calculations. Only the methylene carbons and naphthalene rings were afforded degrees of freedom: all other atoms were held fixed. Single-point energies were calculated using the coordinate driving function at 10° increments, yielding a total of 36 conformational energies. Semiempirical, single-point energy calculations of several of these conformations were also performed using the RHF/PM3(tm) method. Qualitatively similar results were obtained at both levels of theory.

Results and Discussion

Structure and Basic Physical Properties of $[Fe_2(O)(O_2CCH_2C_{10}H_7)_2(TACN\text{-}Me_3)_2](PF_6)_2$. The choice of naphthalene as a donor for this system was largely motivated by the ready availability of 2-naphthylacetic acid and the fact that the photophysics of naphthalene has been thoroughly documented.[28,34−44] To further simplify these initial photophysical studies, we also replaced Tp with TACN-Me_3 as the capping ligand for the cluster.[45] The synthesis of $[Fe_2(O)(O_2CCH_2C_{10}H_7)_2(TACN\text{-}Me_3)_2](PF_6)_2$ (**3**) was accomplished using modified literature procedures[23] and proceeded with good yield. X-ray quality crystals were grown by slow evaporation of CH_2Cl_2 at −20 °C. Details about the structure can be found in Table 1 and in the Supporting Information. A thermal ellipsoid plot of **3** is shown in Figure 1 with selected bond lengths and angles listed in Table 2. Bond lengths and angles associated with the iron−oxo core are all unremarkable and similar to those reported in the literature for this class of high-spin ferric compounds.[23] For example, the average $Fe—O_{bridge}$ bond length in **3** is 1.80(1) Å, the Fe···Fe distance is 3.13(2) Å, and the $Fe—O_{bridge}—Fe$ angle is 120.8(2)°: this can be compared with $[Fe_2(O)(O_2CCH_3)_2(TACN\text{-}Me_3)_2](PF_6)_2$ which has corresponding distances of 1.800(3) and 3.120(3) Å, and an $Fe—O_{bridge}—Fe$ angle of 119.7(2)°.[22] The distinguishing feature of complex **3** is the presence of the naphthalene rings associated with the bridging carboxylates. Metric details within the rings are

(32) The *y*-value offset was allowed to vary during the fit of the data in order to account for random noise (usually 10−60 counts) detected during the experiment.

(33) *Spartan*, 5.0 ed.; Wavefunction, Inc.: Irvine, CA, 1995.
(34) Berlman, I. B. *Handbook of Fluorescence Spectra of Aromatic Molecules*, 2nd ed.; Academic Press: New York, 1971.
(35) Bernhardt, P. V.; Moore, E. G.; Riley, M. J. *Inorg. Chem.* **2001**, *40*, 5799−5805.
(36) Birks, J. B. *Photophysics of Aromatic Molecules*; Wiley-Interscience: New York, 1970.
(37) Chandross, E. A.; Dempster, C. J. *J. Am. Chem. Soc.* **1970**, *92*, 3586−3593.
(38) Chandross, E. A.; Dempster, C. J. *J. Am. Chem. Soc.* **1970**, *92*, 704−706.
(39) Dabestani, R.; Ivanov, I. N. *Photochem. Photobiol.* **1999**, *70*, 10−34.
(40) East, A. L.; Lim, E. C. *J. Chem. Phys.* **2000**, *113*, 8981−8993.
(41) Goryaeva, E. M.; Shablya, A. V.; Ermolaev, V. L. *Opt. Spectrosc.* **2001**, *99*, 508−515.
(42) Kawai, A.; Okutsu, T.; Obi, K. *Chem. Phys. Lett.* **1995**, *235*, 450−455.
(43) Saigusa, H.; Azumi, T. *J. Chem. Phys.* **1980**, *72*, 1713−1715.
(44) Yanagidate, M.; Takayama, K.; Takeuchi, M.; Nishimura, J.; Shizuka, H. *J. Phys. Chem.* **1993**, *97*, 8881−8888.

(45) Intimate control over the magnitude of exchange coupling is not as straightfoward for TACN-Me_3 capped complexes due to the deprotonation of the hydroxo bridge in CH_3CN solution. Although it is possible to make the solution acidic in order to stabilize the complex, all acids used either decomposed the sample (HCl, H_2SO_4) or absorbed light at the same wavelengths as naphthalene ($HClO_4$).

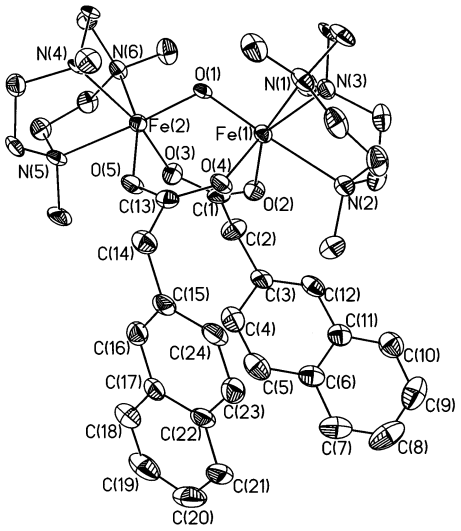

Figure 1. Drawing of $[Fe_2(O)(O_2CCH_2C_{10}H_7)_2(TACN\text{-}Me_3)_2](PF_6)_2$ (**3**) obtained from a single-crystal X-ray structure determination, shown as 50% thermal ellipsoid representation. The hydrogen atoms, two PF_6^- counterions, and CH_2Cl_2 solvate have been omitted for clarity.

Table 2. Selected Bond Distances (Å) and Angles (deg) for $[Zn_2(OH)(O_2CCH_2C_{10}H_7)_2(TACN\text{-}Me_3)_2](ClO_4)$ (**2**) and $[Fe_2(O)(O_2CCH_2C_{10}H_7)_2$ $(TACN\text{-}Me_3)_2](PF_6)_2$ (**3**)

	2 (M = Zn)	**3** (M = Fe)
	Bond Distances (Å)	
M1−O1	2.001(2)	1.802(3)
M2−O1	2.003(2)	1.798(4)
M1−O2	2.115(2)	2.007(4)
M1−O4	2.093(2)	2.027(4)
M2−O3	2.115(2)	2.030(4)
M2−O5	2.065(2)	2.041(4)
M1−N1	2.260(2)	2.171(4)
M1−N2	2.245(2)	2.282(4)
M1−N3	2.250(2)	2.191(5)
M2−N4	2.235(2)	2.183(4)
M2−N5	2.296(2)	2.263(5)
M2−N6	2.252(2)	2.186(4)
M1···M2	3.37	3.13
C5−centroid[a]	10	∼4
centroid−centroid[b]	12	6
	Bond Angles (deg)	
M1−O1−M2	114.57(8)	120.8(2)
O1−M1−O2	94.78(7)	97.0(2)
O2−M1−O4	96.10(7)	94.0(2)
O1−M1−O4	96.32(7)	97.3(2)
O1−M2−O3	97.96(7)	96.8(2)
O1−M2−O5	94.68(7)	96.9(2)
O3−M2−O5	96.00(7)	93.9(2)

[a] The centroid here refers to the center of the six-membered ring containing atom C15. [b] Calculated from midpoint of the C6−C11 bond to the midpoint of C18−C27 bond.

as expected; for example, carbon−carbon bonds have average lengths of 1.39(5) Å (longest 1.439 Å; shortest 1.346 Å). In terms of their relative position, the planes of the naphthyl moieties (deviation from planarity 0.0094 Å) are oriented nearly perpendicular to each other (72.4°). The closest contact exists between the center of the six-membered ring containing C15 on one naphthalene group and the C5 atom on the other: at 4 Å, this distance is close enough for the hydrogen atom of one naphthalene to interact with the π-system of the other. Inspection of the packing diagram did not reveal any significant intermolecular interactions between adjacent dinuclear iron clusters.

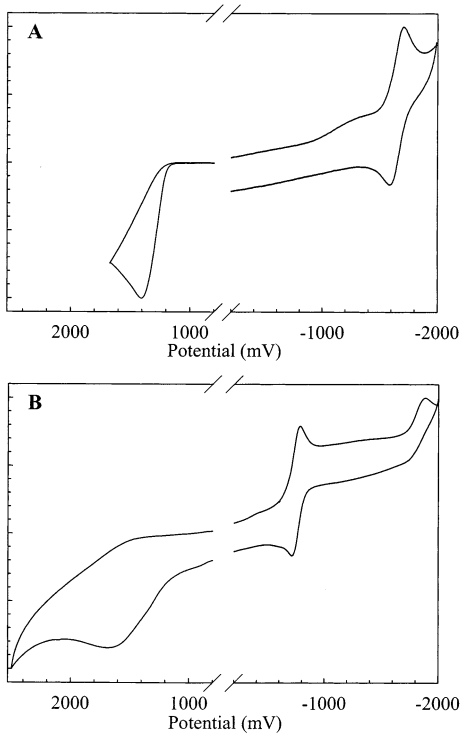

Figure 2. Cyclic voltammograms for (A) methyl-2-naphthylacetate (**1**) and (B) $[Fe_2(O)(O_2CCH_2C_{10}H_7)_2(TACN\text{-}Me_3)_2](PF_6)_2$ (**3**) both in acetonitrile. Potentials are reported relative to $Ag/AgNO_3$. See text for further details.

Electrochemistry. The electrochemical properties of methyl-2-naphthylacetate (**1**), $[Zn_2(OH)(O_2CCH_2C_{10}H_7)_2$-$(TACN\text{-}Me_3)_2](ClO_4)$ (**2**), and $[Fe_2(O)(O_2CCH_2C_{10}H_7)_2$ $(TACN\text{-}Me_3)_2](PF_6)_2$ (**3**) were examined using cyclic voltammetry; data for compounds **1** and **3** are shown in Figure 2. The assignment of the redox behavior of **3** was based largely upon comparison with the cyclic voltammograms of **1** and **2**. Compound **1** shows a reversible reduction corresponding to formation of the radical anion with $E_{1/2} = -1.60$ V. In contrast, oxidation of **1** is irreversible at a potential of +1.4 V. Because the Zn^{II} centers of compound **2** are not expected to be redox-active, the irreversible oxidation at +1.5 V and the quasireversible reduction at −1.8 V can likewise be assigned to the naphthalene moiety of this bridged dinuclear cluster. The presence of Fe^{III} is expected to complicate the redox properties of **3**. Indeed, we observe a total of three redox waves for compound **3**: two reductive and one oxidative. On the basis of the observations for compounds **1** and **2**, we assign the irreversible waves at −1.9 and +1.65 V to reduction and oxidation, respectively, of the naphthalene group. Accordingly, the reversible one-electron reduction with $E_{1/2} = -0.75$ V is assigned as the Fe^{III}/Fe^{II} redox couple. This latter assignment is further supported by electrochemical data on $[Fe_2(O)(O_2CCH_3)_2(TACN\text{-}Me_3)_2](PF_6)_2$ which displays a similar feature at −0.64 V versus $Ag/AgNO_3$ in CH_2Cl_2.[23]

Magnetism. Variable temperature magnetic susceptibility data for **3** are shown in Figure 3. The compound exhibits an effective moment of ∼3 μ_B at 380 K which decreases with decreasing temperature to a value of ∼1 μ_B at 5 K. The antiferromagnetic coupling implied by these observations can

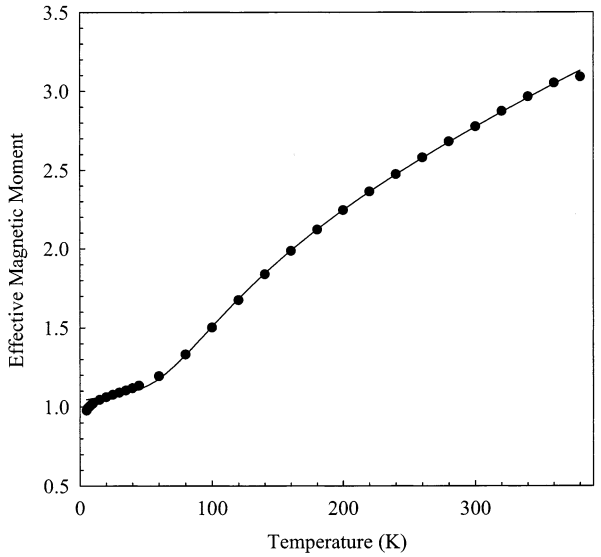

Figure 3. Plot of effective magnetic moment versus temperature for $[Fe_2(O)(O_2CCH_2C_{10}H_7)_2(TACN\text{-}Me_3)_2](PF_6)_2$ (**3**, ●) in the solid state. The solid line represents the theoretical fit of the data. See text for further details.

be quantified by fitting the data to a spin Hamiltonian of the form

$$\mathbf{H} = -2J\mathbf{S}_1\cdot\mathbf{S}_2 \qquad (4)$$

where $\mathbf{S}_1$ and $\mathbf{S}_2$ are the single-ion spin operators for Fe(1) and Fe(2), respectively, and J is the scalar exchange integral. The solid line in Figure 3 represents a fit of these data to an operator-equivalent form of eq 4 with $J = -105$ cm^{-1}.[46] This value is similar to that found for other members of this class of compounds.[23] In addition, the magnetic susceptibility of **3** was determined via the Evans method in order to assess the integrity of the dinuclear complex in solution. A value of 2.9 ± 0.1 μ_B was found at 300 K. This value compares favorably to the value of 2.8 μ_B observed in the solid state and is significantly lower than the uncoupled value of 8.37 μ_B, establishing that the bridged core stays intact in solution.

Ground-State Absorption. The electronic absorption spectrum of **3** is illustrated in Figure 4. All of the features observed in the visible and near-UV are endemic to the iron−oxo core. For example, transitions at 350, 475, and 522 nm are assigned as ligand-to-metal charge transfer (LMCT) bands associated with the bridging oxide.[47] In addition, a formally forbidden d−d transition is observed at 740 nm (not shown) which gains intensity due to the exchange interaction between the two high-spin Fe^{III} centers.[48] Features in the UV ($\lambda < 300$) are best described in terms of a superposition of bands characteristic of the iron−oxo core and absorptions due to the naphthalene groups. The shoulders near 280 nm in the spectrum of **3** are consistent with the vibrational fine

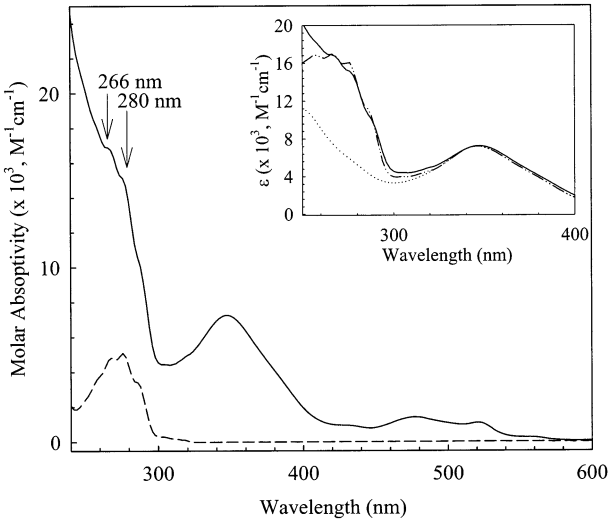

Figure 4. Absorption spectra of methyl-2-naphthylacetate (**1**, - - -) and $[Fe_2(O)(O_2CCH_2C_{10}H_7)_2(TACN\text{-}Me_3)_2](PF_6)_2$ (**3**, —) in acetonitrile at 298 K. The arrows indicate the excitation wavelengths used. The inset shows an overlay of the absorption spectrum of **3** along with $[Fe_2(O)(O_2CCH_3)_2(TACN\text{-}Me_3)_2](PF_6)_2$ (···) and a spectrum corresponding to a linear sum of $[Fe_2(O)(O_2CCH_3)_2(TACN\text{-}Me_3)_2](PF_6)_2$ and methyl-2-naphthylacetate (-···-).

structure seen in compound **1** and assigned as $\pi^* \leftarrow \pi$ transitions of the naphthalene.[36] The inset of Figure 4 shows that the spectrum of **3** can be represented by summing the molar absorbtivities of $[Fe_2(O)(O_2CCH_3)_2(TACN\text{-}Me_3)_2](PF_6)_2$ and **1**, indicating that the electronic coupling between the core and the naphthalene rings in the ground state of compound **3** is relatively weak.

Static and Time-Resolved Spectroscopies. Static emission spectra of methyl-2-naphthylacetate (**1**), $[Zn_2(OH)(O_2CCH_2C_{10}H_7)_2(TACN\text{-}Me_3)_2](ClO_4)$ (**2**), and $[Fe_2(O)(O_2CCH_2C_{10}H_7)_2(TACN\text{-}Me_3)_2](PF_6)_2$ (**3**) were obtained at 298 K in CH_3CN and are plotted in Figure 5. The spectral profiles for compounds **1** and **2** are very similar, suggesting that there is very little change in the emissive properties of the naphthalene group upon chelation to the Zn^{II}_2 core. On the basis of both the spectral profile and the observed lifetime (vide infra), the emission is assigned as fluorescence from naphthalene.[34] The radiative quantum yields for **1** and **2** were determined to be 0.13 and 0.14, respectively. Phosphorescence, which is sometimes observed for substituted naphthalenes, was not detected. The emission spectrum of compound **3**, however, displays some striking differences. The overall intensity of the emission is attenuated by roughly a factor of 10 relative to that of both **1** and **2**. In addition, the spectrum is significantly broadened on the low energy portion of the emission envelope. This near-ultraviolet broadening is not characteristic of naphthalene phosphorescence, which typically appears as a weak, relatively structured emission in the mid-visible region.[36] The overall attenuation of emission was promising in that it suggested the presence of a competing process which was quenching the naphthalene fluorescence (e.g., electron transfer to the iron−oxo core which has a calculated driving force of $\Delta G = -1.7$ eV[49]). Therefore, the nature of the emission from compound **3** was examined more closely.

(46) Values for g and contributions from temperature independent paramagnetism (TIP) were held fixed at 2.00 and 4.0×10^{-4} cgs, respectively. In addition, a trace amount (3%) of paramagnetic impurity, evident from the data at low temperature, was also incorporated into the model.

(47) Brown, C.; Remar, G.; Musselman, R.; Solomon, E. *Inorg. Chem.* **1995**, *34*, 688−717.

(48) McCarthy, P.; Gudel, H. *Coord. Chem. Rev.* **1988**, *88*, 69−131.

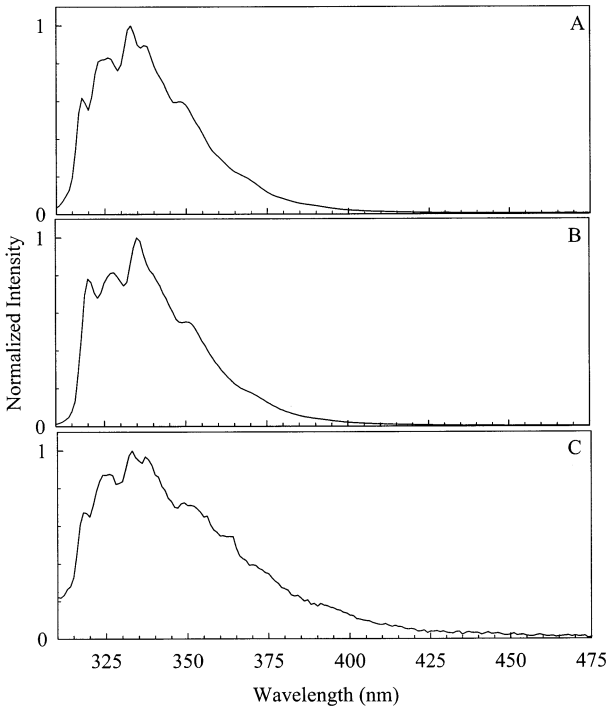

Figure 5. Corrected emission spectra for (A) methyl-2-naphthylacetate (**1**), (B) $[Zn_2(OH)(O_2CCH_2C_{10}H_7)_2(TACN\text{-}Me_3)_2](ClO_4)$ (**2**), and (C) $[Fe_2(O)(O_2CCH_2C_{10}H_7)_2(TACN\text{-}Me_3)_2](PF_6)_2$ (**3**) in deoxygenated acetonitrile at room temperature. All samples were excited at 280 nm.

Both methyl-2-naphthylacetate (**1**) and $[Zn_2(OH)(O_2CCH_2C_{10}H_7)_2(TACN\text{-}Me_3)_2](ClO_4)$ (**2**) show monophasic emission kinetics (Figure 6, inset) with lifetimes of 58 ± 1 and 47 ± 1 ns, respectively. Given the measured emission quantum yield for **1**, we calculate radiative (k_r) and nonradiatvie (k_{nr}) decay rates of 2.2×10^6 and 1.5×10^7 s^{-1}, respectively. Both of these rates are slightly larger for the Zn complex, with $k_r = 3.0 \times 10^6$ s^{-1} and $k_{nr} = 1.8 \times 10^7$ s^{-1}. The reduced lifetime of the naphthalene $S_0 \leftarrow S_1$ transition in compound **2** is therefore due to these small increases in both k_r and k_{nr}. However, these data confirm that the Zn^{II} ions have little effect on the photophysics of naphthalene. In contrast to the monophasic kinetics observed for **1** and **2**, $[Fe_2(O)(O_2CCH_2C_{10}H_7)_2(TACN\text{-}Me_3)_2](PF_6)_2$ (**3**) exhibits biphasic emission (Figure 6) with lifetimes of $\tau_1 = 4.6 \pm 1$ ns and $\tau_2 = 49 \pm 1$ ns. The biphasic kinetics rule out a simple dynamic quenching model to explain the attenuated emission intensity and, instead, suggest the presence of two distinct, kinetically uncoupled emissive species. The value of τ_2 is within experimental error of the lifetime measured for complex **2**, suggesting that this component is likely due to the $S_0 \leftarrow S_1$ transition of naphthalene. The fast decaying species observed for **3**, however, is clearly new: its lifetime is significantly shorter than τ_2 and not at all characteristic of naphthalene molecules in solution.

(49) $\Delta G = (E_{ox,nap} - E_{red,Fe}) - E_{00} - CSE$ where $E_{ox,nap}$ is the oxidation potential for **1** (1.4 V) and $E_{red,\,Fe}$ is the $E_{1/2}$ for the $Fe^{III/II}$ redox couple in **3** (−0.75 V), E_{00} is the zero-point energy of the donor which is estimated from the emission maximum of **1** (3.76 eV), and CSE is the Coulomb stabilization energy for the charge separated species. $CSE = e^2/\epsilon r$ where e is the electron charge, ϵ is the dielectric constant of CH_3CN (37.5), and r is the distance between the donor and acceptor (6.9 Å). For a detailed discussion of this equation see: Oevering, H.; Paddon-Row, M. N.; Heppener, M.; Oliver, A. M.; Cotsaris, E.; Verhoeven, J. W.; Hush, N. S *J. Am. Chem. Soc.* **1987**, *109*, 3258−3269.

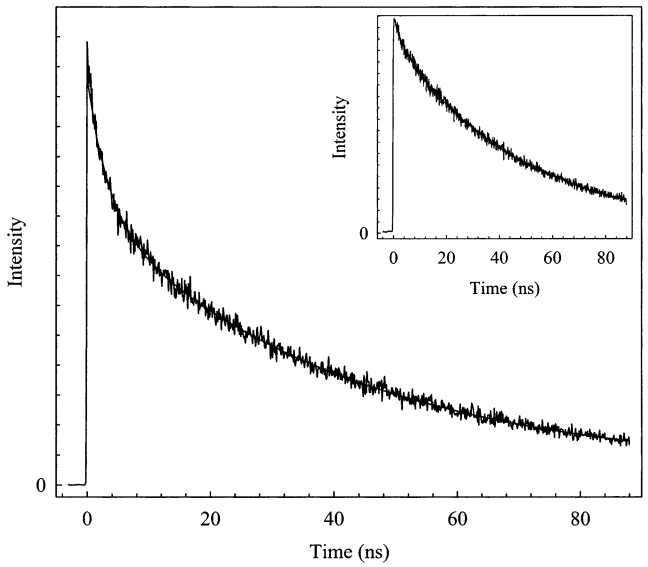

Figure 6. Time-resolved emission data for $[Fe_2(O)(O_2CCH_2C_{10}H_7)_2(TACN\text{-}Me_3)_2](PF_6)_2$ (**3**) at 360 nm following ca. 30 ps excitation at 280 nm. The solid line is a fit to a biexponential decay model with $\tau_1 = 4.6 \pm 1$ ns and $\tau_2 = 49 \pm 1$ ns. The inset shows corresponding data for $[Zn_2(OH)(O_2CCH_2C_{10}H_7)_2(TACN\text{-}Me_3)_2](ClO_4)$ (**2**) at 360 nm. These data can be fit to a single-exponential model with $\tau = 47 \pm 1$ ns.

Emission anisotropy data lend further support to the notion that two distinct chemical species give rise to the biphasic emission of **3**. Whereas the described magic angle data provide information on population dynamics (i.e., excited-state lifetimes), emission anisotropy measurements probe dynamics associated with the orientation of the transition dipole. Initially, emission will be polarized parallel to the emission dipole and will therefore be anisotropic for point group symmetries lower than cubic. This anisotropy will disappear as chemical and/or physical processes (e.g., molecular rotation) ensue, eventually yielding an isotropic signal where $r(t) = 0$ (eq 2). The value of $r(0)$, the initial anisotropy, is diagnostic for the orientation and degeneracy of the emission dipole (eq 3). Both **1** and **2** exhibited instrument-limited anisotropy decays, indicating depolarization times of <30 ps. Compound **3**, however, displayed significantly different anisotropy behavior than either of the two model compounds (Figure 7). The data can be fit to a biexponential decay model with time constants of $\tau_a = 56 \pm 20$ ps and $\tau_b = 1.4 \pm 0.4$ ns; the corresponding initial amplitudes are 0.23 ± 0.1 and 0.06 ± 0.04, respectively. Using eq 3, these results indicate that there are two distinct transition dipoles, whose anisotropies decay at different rates, oriented at angles of $32 \pm 10°$ (τ_a) and $49 \pm 5°$ (τ_b) relative to the excitation polarization. Whether the 56 ps anisotropy decay corresponds to the instrument-limited dynamics of **1** and **2** cannot be stated with certainty. However, the 1.4 ns component clearly represents a photophysical feature unique to compound **3**.

Given the evidence for two emitting species associated with compound **3**, we sought to acquire time-gated emission spectra to deconvolve their contributions to the spectrum

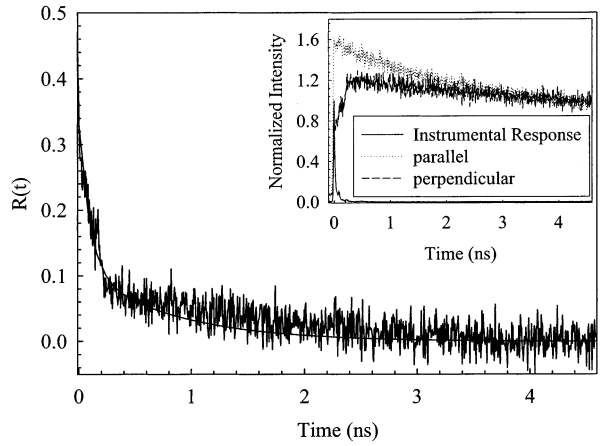

Figure 7. Time-resolved emission anisotropy data, plotted as $r(t)$, for $[Fe_2(O)(O_2CCH_2C_{10}H_7)_2(TACN\text{-}Me_3)_2](PF_6)_2$ (**3**). The solid line is a fit to a biexponential decay model with $\tau_a = 0.056 \pm 0.020$ ns and $\tau_b = 1.4 \pm 0.4$ ns. The inset shows the parallel ($I_{||}$) and perpendicular ($I_\perp$) polarized emission data used to calculate $r(t)$, along with a plot of the instrument response function.

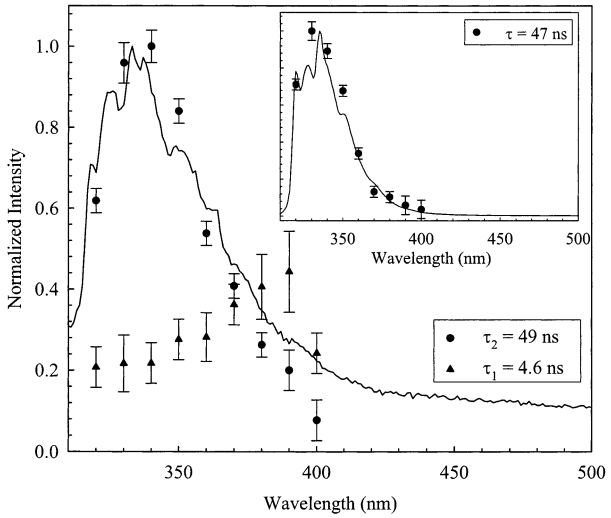

Figure 8. Gated emission spectra of $[Fe_2(O)(O_2CCH_2C_{10}H_7)_2(TACN\text{-}Me_3)_2](PF_6)_2$ (**3**) and $[Zn_2(OH)(O_2CCH_2C_{10}H_7)_2(TACN\text{-}Me_3)_2](ClO_4)$ (**2**, inset). The plots show the normalized static emission spectrum (—) in CH_3CN superimposed on the TCSPC emission amplitudes obtained from fits of the data at each probe wavelength. See text for further details.

shown in Figure 5C. This is typically done by simply plotting the amplitude of the decay (i.e., $I(0)$ from the fit) as a function of probe wavelength. However, to have internally consistent data across each gated spectrum, variations in the detection efficiency of the monochromator at different wavelengths were corrected for by scaling the emission decay curves for **1** at all probe wavelengths to the compound's static emission spectrum (see Experimental Section). This process allowed a scaling factor to be determined for each probe wavelength in the time-resolved experiment. The scaled preexponentials were then normalized and plotted against the normalized static emission spectrum of the compound. The emission spectrum obtained in this manner for compound **2** is illustrated in the inset of Figure 8 along with its corrected emission spectrum from Figure 5B. The agreement between the two is quite good, giving us confidence in the validity of this approach.

The preexponentials for the long time component of compound **3** shown in Figure 8 reveal a spectrum consistent with the $S_0 \leftarrow S_1$ fluorescence of naphthalene. In contrast, the 4.6 ns component exhibits a spectral profile which is significantly broadened and red-shifted relative to that observed for either **1** or **2**. By inspection, it is clear that a superposition of these two contributions recovers the static spectrum of compound **3**. We therefore assert that the low energy broadening noted in Figure 5C is due to the presence of this short-lived emissive species.

The spectral signature of the 4.6 ns species is characteristic of an excimer. Aromatic chromophores such as naphthalene are well-known to form emissive excited-state dimers under appropriate conditions.[36] For example, 1,3-di(2-naphthyl)-propane has been investigated by E. A. Chandross et al.[37] This compound exhibits two distinct emissive characteristics: one assigned as fluorescence centered at ~330 nm and the other assigned as excimer emission centered at ~390 nm. Complex **3** is strikingly similar with one component centered at 340 nm ($\tau_2 = 49 \pm 1$ ns) and the other centered at ~390 nm ($\tau_1 = 4.6 \pm 1$ ns). As in 1,3-di(2-naphthyl)-propane, the band centered at 390 nm in **3** is broad and red-shifted relative to the monomer fluorescence.

The 4.6 ns lifetime is unusual in that excimer emission is generally longer lived than the corresponding monomer fluorescence.[36] Several possible explanations for this can be considered. Because neither of the observed emission lifetimes for compound **3** was found to be concentration dependent, at least over the range 10^{-5} to 10^{-6} M, a bimolecular quenching process can be immediately ruled out. Intramolecular quenching, for example, via energy and/or electron transfer from the naphthalene excimer to the iron–oxo core, could also account for the short lifetime: this point will be addressed in a following paragraph. In addition to competition from parallel quenching mechanisms, the specific conformation of an excimer has been shown to produce significant variance in the observed emission lifetime. For example, a so-called sandwich conformation for 9,10-dimethylanthracene (i.e., when the molecular planes are cofacial) yields an excimer with a lifetime of ~220 ns whereas two anthracenes whose molecular planes lie at a relative angle of ~55° produce an excimer with a 6 ns lifetime.[36] The excimer lifetime of 2-methylnaphthalene in 95% ethanol is 220 ns, but recent work by Yanagidate et al.[44] has found that lifetimes vary depending on the conformation of naphthalenophanes. Therefore, the 4.6 ns lifetime may be due to the presence of a noncofacial conformation (or distribution of conformations) of the two naphthalene rings in **3**. This would also be consistent with the change in emission dipole orientation relative to that of the naphthalene monomer detected in the anisotropy measurements.

Transient absorption experiments were undertaken in an effort to further characterize the excimer. Samples were excited at 266 nm and monitored from 400 to 700 nm in 20 nm increments. Compound **1** showed biphasic transient absorption kinetics with lifetimes of $\tau_1 = 60 \pm 5$ ns and $\tau_2 = 48 \pm 1$ μs. The two components also had slightly different absorption spectra, the 60 ns species having an absorption

maximum at 420 nm while the long-lived species exhibited a red-shifted spectrum with $\lambda_{max} \sim 430$ nm. The lifetime of the fast component is within experimental error of the $S_0 \leftarrow S_1$ fluorescence lifetime, allowing us to assign this feature to $S_n \leftarrow S_1$ absorption(s) of the singlet excited state of **1**. On the basis of its long lifetime and spectral profile as compared to other reports in the literature,[40−43,50−53] the 48 μs species is assigned as a triplet excited state of **1**, most likely T_1. In contrast to the reasonably strong signals obtained for **1**, transient absorption signals for **3** were found to be extremely weak.[54] However, it was clear that there were no instrument-limited features (i.e., corresponding to the 4.6 ns excimer emission) present at probe wavelengths of $\lambda > 450$ nm.[55] This strongly suggests that the excimer formed in **3** is a singlet, because the triplet excimer is expected to absorb near 600 nm.[50,53,56] The relatively short lifetime for the excimer is therefore quite reasonable in light of this result.

No features attributable to the naphthalene radical cation were observed. The spectrum of this species is expected to be relatively weak; nevertheless, there is no evidence from our data to suggest excited-state electron transfer occurs from the naphthalene to the iron−oxo core. Whether the attenuated emission of **3** is an indication of energy transfer between the two is difficult to state with certainty. We have no quantitative information on the value of k_r for the excimer. If it is smaller than that of the monomer, then the overall emission intensity will be expected to decrease concomitant with excimer formation. The LMCT feature of the Fe_2O core near 350 nm likely reabsorbs some of the emission from the naphthyl group in **3**. Given the dilute conditions under which the data were collected, this internal filtering effect should be quite small. However, the spectral overlap which facilitates this filtering predisposes the system for efficient Förster transfer from the naphthalene to the iron−oxo core. This same situation will be operative for the excimer, as well. It, therefore, seems likely that excimer formation and energy transfer both contribute to the overall reduction in emission intensity observed for complex **3**. The latter may also be a factor in determining the relatively short observed lifetime of the excimer.

Structure of $[Zn_2(OH)(O_2CCH_2C_{10}H_7)_2(TACN\text{-}Me_3)_2](ClO_4)$ (2). The final point we wish to discuss is the interesting result that a short-time component is not observed for **2** even though the two bridging 2-naphthylacetates could interact in a similar manner as in **3**. Thus, a single-crystal X-ray structure determination was carried out in order to assess whether there were any significant structural variations in **2** which would account for the lack of excimer formation. Details about the structure can be found in Tables 1 and 2; a thermal ellipsoid plot of **2** is shown in Figure 9. The bond lengths and angles are similar to compounds of this class[22] with an average Zn−OH(bridge) bond length of 2.002(2) Å and a Zn−OH−Zn angle of 114.57(8)°. This bridging angle is slightly more acute than that observed for **3** (120.8°); however, the longer bond lengths still yield a Zn···Zn distance of 3.37 Å compared to the Fe···Fe distance of 3.13 Å in **3**. Structural parameters within each naphthalene group are unremarkable. However, in stark contrast to the naphthalene−naphthalene interactions evident in complex **3**, the closest carbon−carbon distance between the two bridging naphthylacetates in the Zn^{II} analogue is over 8 Å. Hence, no intramolecular interactions between the naphthyl groups are apparent. The packing diagram for **2**, likewise, shows no obvious interactions between naphthalene rings on adjacent dinucluear zinc clusters. Unlike the corresponding iron complex, the naphthyl groups in complex **2** appear to be well isolated.

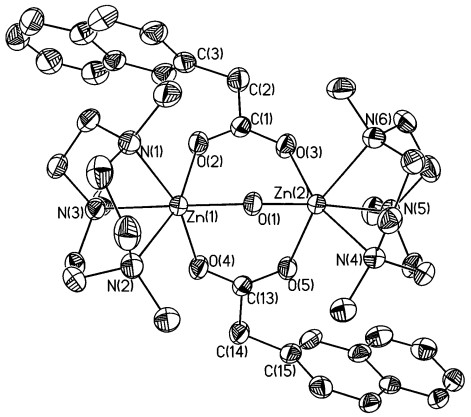

Figure 9. Drawing of $[Zn_2(OH)(O_2CCH_2C_{10}H_7)_2(TACN\text{-}Me_3)_2](ClO_4)$ (**2**) obtained from a single-crystal X-ray structure determination shown as a 50% thermal ellipsoid representation. The hydrogen atoms, ClO_4^- counterion, and CH_3OH solvate have been omitted for clarity. The numbering scheme is identical to $[Fe_2(O)(O_2CCH_2C_{10}H_7)_2(TACN\text{-}Me_3)_2](PF_6)_2$ (**3**) in Figure 1.

Packing forces in the solid state could clearly be influencing the relative conformation of the bridging naphthalene groups. A molecular dynamics simulation was therefore undertaken to gain further insight into the energetics associated with conformational changes of the two naphthyl groups. The calculations were performed by importing the crystal structure into the Spartan 5.0 software program[33] and freezing all atoms except those associated with the naphthalene groups. The bond between C1 and C2 or C13 and C14 was allowed to rotate by changing the dihedral angle between the two naphthalene rings. Zero-point energies were then calculated for several conformations as the two naphthalene rings went from an eclipsed geometry to one in which they were as far apart as possible. The calculations bore similar results for both **2** and **3**. Not surprisingly, the lowest energy conformation was one for which the two naphthalene rings were essentially cofacial, presumably the result of $\pi-\pi$

(50) Lim, E. C.; Subudhi, P. C. *Chem. Phys. Lett.* **1978**, *56*, 59−61.
(51) Lim, E. C. *Acc. Chem. Res.* **1987**, *20*, 8−17.
(52) Saigusa, H.; Azumi, T. *J. Chem. Phys.* **1979**, *71*, 1408−1413.
(53) Wang, X.; Kofron, W. G.; Kong, S.; Rajesh, C. S.; Modarelli, D. A.; Lim, E. C. *J. Phys. Chem. A* **2000**, *104*, 1461−1465.
(54) Multiphasic transient absorption kinetics were also observed for compound **2**. The fastest component had a lifetime of $\tau_1 = 53 \pm 4$ ns and was assigned as in compound **1** to the S_1 state of naphthalene. Long-lived components with $\tau_2 = 12 \pm 1$ μs and $\tau_3 = 51 \pm 4$ μs were also observed. Although the lifetimes suggest organic triplets (e.g., T_1), the presence of two components as opposed to the one found for **1** is still under investigation.
(55) Although the FWHM of the instrument response function for our nanosecond spectrometer is 13 ns, species with lifetimes as short as 700 ps are still observable as pulsewidth-limited features.
(56) Terazima, M.; Cai, J.; Lim, E. C. *J. Phys. Chem. A* **2000**, *104*, 1662−1669.

interactions between the two ring systems; the zero-point energy was slightly higher when the two rings were far apart. However, the calculation also revealed a high energy barrier associated with rotation of the naphthalene rings past the TACN-Me_3 groups. Similar results were found using semiempirical methods (PM3(tm)) where the zero-point energies for several discrete conformations of the naphthalene rings were calculated. This result suggests that excimer formation in complex **2** will be more difficult than in complex **3**: the naphthalene rings in **2** must rotate past the TACN-Me_3 in order to interact, whereas in **3** they are in a conformation which can produce an excimer in the absence of such large amplitude motion. While these results do not constitute proof that the solid-state structure for **2** reflects the molecule's conformation in solution, they are certainly consistent with the surprising difference in the photophysical behavior observed for the two compounds.

Concluding Comments

This paper has described the synthesis, structure and physical properties of an intramolecular donor/acceptor system. The compound that was synthesized, $[Fe_2(O)(O_2CCH_2C_{10}H_7)_2(TACN\text{-}Me_3)_2](PF_6)_2$ (**3**), consists of an oxo-bridged dinuclear core of antiferromagnetically coupled high-spin Fe^{III} ions appended with two naphthylacetate groups. The original intention was to monitor electron and/or energy transfer from the naphthalene into the iron−oxo core. However, upon photoexcitation of the naphthalene moiety, it was found that the molecule presented complicated emission behavior not at all characteristic of the simple quenching that had been expected. Use of a variety of spectroscopic probes helped to determine that the unexpected twist in the photophysics of this compound arises from an excimer that forms between the two naphthyl groups. The relatively short lifetime of the excimer (4.6 ns) is believed to be due to its singlet character coupled with a noncofacial geometry. Possible contributions from energy transfer from the excimer to the iron−oxo core have also been noted. The existence of this excimer is no doubt a consequence of the structure imposed by the oxo-bis-carboxylato motif. Whether its formation in this compound is in part responsible for the lack of any clear evidence for electron transfer between the naphthalene groups and the spin-coupled cluster is not known. However, the possibility of excimer dynamics is clearly a factor that will have to be considered in future designs of intramolecular donor/acceptor assemblies of this type.

Acknowledgment. The authors would like to thank Professor Gary Blanchard for use of the time-correlated single-photon counting system and for help with the experimental setup. Dr. Edward Byrd is also gratefully acknowledged for helpful discussions concerning the molecular dynamics simulations.

Supporting Information Available: Crystallographic data (PDF, CIF). This material is available free of charge via the Internet at http://pubs.acs.org.

IC026054M